Available online at www.sciencedirect.com
SCIENCE DIRECT®
International Journal of Solids and Structures 43 (2006) 3006–3024
INTERNATIONAL JOURNAL OF SOLIDS and STRUCTURES
www.elsevier.com/locate/ijsolstr

Bending and local buckling of a nanocomposite beam reinforced by a single-walled carbon nanotube

T. Vodenitcharova, L.C. Zhang *

School of Aerospace, Mechanical and Mechatronic Engineering, The University of Sydney, NSW 2006, Australia

Received 1 February 2005; received in revised form 18 May 2005
Available online 5 July 2005

Abstract

This paper studies the pure bending and bending-induced local buckling of a nanocomposite beam reinforced by a single-walled carbon nanotube (SWNT). The Airy stress-function method was employed to analyse the deformation of the matrix, and the cross-sectional change of the SWNT in bending was taken into account. A particular consideration was given to the effect of the SWNT's radial flexibility on the strain/stress states and buckling. It was found that in thicker matrix layers the SWNT buckles locally at smaller bending angles and greater flattening ratios. This causes higher strains/stresses in the surrounding matrix and in turn degrades the strength of the nanocomposite structure.

Keywords: Single-walled carbon nanotubes; Nanocomposites; Local buckling in pure bending

1. Introduction

The high strength and stiffness of carbon nanotubes have generated enormous interest in the scientific community in recent years (Thostenson et al., 2001; Dai, 2002; Salvetat-Delmotte and Rubio, 2002). One of the areas has been the applicability of carbon nanotubes as a reinforcing constituent (Lourie et al., 1998; Schadler et al., 1998; Wagner et al., 1998; Shaffer and Windle, 1999; Qian et al., 2000; Cooper et al., 2002; Lau and Shi, 2002; Barber et al., 2003; Liu and Chen, 2003; Thostenson and Chou, 2003; Tai et al., 2004) and it has been found that the addition of a small percentage of nanotubes in a matrix may considerably increase the composite's mechanical strength and fracture toughness (Qian et al., 2000). However,

* Corresponding author. Tel.: +61 2 9351 2835; fax: +61 2 9351 7060.
E-mail address: zhang@aeromech.usyd.edu.au (L.C. Zhang).

0020-7683/$ - see front matter
doi:10.1016/j.ijsolstr.2005.05.014

Nomenclature

L length of the nanocomposite beam (Fig. 1)
ψ, M bending angle and bending moment, respectively (Fig. 1)
t_{NT}, t_m thicknesses of the SWNT wall and the surrounding matrix layer, respectively (Fig. 1)
R_{NT}, R_m mid-radius of the SWNT and outer radius of matrix, respectively (Fig. 1)
E_{NT}, E_m Young's modulii of the SWNT and matrix, respectively
G_m shear modulus of matrix
μ_{NT}, μ_m Poisson's ratios of SWNT and matrix, respectively
r, θ polar coordinates (Fig. 1)
U_f, U_l energies of the nanocomposite beam of a unit length in flattening and in longitudinal stretching, respectively
U total energy of the nanocomposite beam of a unit length, $U_f + U_l$
$C = \psi/L$ curvature of the nanocomposite beam axis
c normalized curvature of the nanocomposite beam axis
ζ_{NT}, ζ_m flattening ratios of the SWNT and the outer surface of the matrix, respectively
w_{NT}, v_{NT} radial and tangential displacements at a point on the SWNT mid-surface (Fig. 1)
w_m, v_m radial and tangential displacements at a point in the matrix (Fig. 1)
η_m distance of a point in the matrix to the neutral axis of the nanocomposite beam, $\theta = 0°$ (Fig. 1)
$k_{\theta\theta,NT}$, $k_{\theta\theta,m}$ circumferential curvature change of the SWNT mid-surface and a matrix fibre, respectively
$\varepsilon^e_{\theta\theta,NT}$, v^e_{NT} circumferential direct strain and displacement, respectively, at a point at the interface between the SWNT and the matrix
$\sigma_{rr,m}$, $\sigma_{\theta\theta,m}$ and $\tau_{r\theta,m}$ stresses at a point in the matrix in polar coordinates
$\varepsilon_{rr,m}$, $\varepsilon_{\theta\theta,m}$, $\varepsilon_{zz,m}$ and $\gamma_{r\theta,m}$ strains at a point in the matrix in polar coordinates
F Airy stress function
$\overline{A}$, $\overline{B}$, $\overline{C}$ and $\overline{D}$ coefficients in the Airy stress function (Eq. (8))
$\sigma_{cr,0,NT}$, $\sigma_{cr,0,m}$ classical buckling stress of the SWNT and matrix, respectively, in uniaxial compression if no flattening is considered
$M_{cr,0,NT}$ bending moment of the nanocomposite beam when the compressive stress in the extreme fibre of the SWNT is $\sigma_{cr,0,NT}$
$\sigma_{cr,NT}$, $\sigma_{cr,m}$ buckling stress of the SWNT and matrix, respectively, in uniaxial compression if flattening is considered
ρ_{NT}, ρ_m local curvature radius of the SWNT mid-surface and the matrix fibre, respectively, at the point of largest compressive stress if flattening is considered
s non-dimensional stress component normalized by $\sigma_{cr,0,NT}$
m non-dimensional bending moment normalized by $M_{cr,0,NT}$

there was also a debate upon the effectiveness of nanotubes in polymer-based structures. Some studies found a weak bond between carbon nanotubes and their surrounding polymer matrix so that the nanotubes could be pulled out easily and, thus, the cavities that the nanotubes occupied could lead to a lower flexural strength of a nanotube/epoxy beam compared with that made of pure epoxy (Lau and Hui, 2002; Lau and Shi, 2002). Many others, however, argued that carbon nanotubes develop a high-strength interface with polymer matrix (Barber et al., 2003, 2004). Their pullout and interface adhesion tests on nanotube/polymer revealed a strong covalent bonding and found that the matrix in the vicinity of the nanotube withstood stresses significantly higher than the stresses that would otherwise yield the bulk polymer specimen. Recent quantum mechanics

studies (Mylvaganam and Zhang, 2004a,c) revealed that strong chemical bonds between alkyl radicals and carbon nanotubes (especially of small diameters) were energetically favourable and that such reaction could take place at multiple sites. Their study also indicated that polymer–SWNT covalent bonds can be introduced by generating free radicals using generators such as peroxide.

Apart from embedding nanotubes in a polymer matrix, researchers have tried to coat carbon nanotubes by electron-beam deposition of various metals in order to obtain continuous metal nanowires (Zhang et al., 2000) or high-performing composite materials (Chen et al., 2003). They found that titanium, nickel and palladium form uniform coating and good bonding fragmentation of the coating occurred (Zhang et al., 2000). Titanium exhibits the strongest Ti–SWNT interaction that could possibly involve covalent bonding, while gold and aluminium give only a weak bond, perhaps due to van der Waals forces (Zhang et al., 2000). It was also found that nickel–phosphorus coating on carbon nanotubes produced higher wear resistance and lower friction coefficient than nickel–phosphorus–SiC (or graphite) composite coating. It appeared that nanotubes embedded in a copper matrix improved the tribological behaviour of the composite over pure copper (Chen et al., 2003).

One characteristic that could affect the reinforcing property of the carbon nanotubes is their extraordinary radial flexibility. It was found that carbon nanotubes alone are exceptionally flexible and undergo reversible deformation to very high-strain levels in all generic loading types due to their high bond-breaking resistance (Iijima et al., 1996; Yakobson et al., 1996; Gao et al., 1998; Srivastava et al., 1999; Yu et al., 2001; Mylvaganam and Zhang, 2004b). Iijima et al. (1996) studied both experimentally and theoretically the deformation properties of carbon nanotubes bent to large angles and discovered that carbon nanotubes could be bent without significant straining up to a critical angle. At that bending angle a V-shaped kink was initiated and developed upon loading, while the material remained elastic. This phenomenon was successfully modelled by the authors (Vodenitcharova and Zhang, 2004) and the results were in good agreement with the observations of Iijima et al. (1996).

In order to facilitate the development of nanocomposite materials, the stress/strain states in both SWNT and matrix under different loading conditions should be studied. As the first part of the authors' series of studies, the present paper will concentrate on the pure bending of a nanocomposite beam of a circular cross section with a perfect nanotube–matrix bonding. It will report on the significance of the SWNT's ovalisation to the stress/strain development in the nanocomposite beam within the elastic range. Of specific interest is the load-bearing capacity of the nanocomposite beam in relation to the local buckling of the SWNT. The analysis in this study will use the equivalent thickness of the SWNT ($t_{NT} = 0.617$ Å) and the equivalent Young's modulus ($E_{NT} = 4.88$ TPa) recently revealed by the authors (Vodenitcharova and Zhang, 2003). These parameters are different from the commonly assumed values in the literature based on a postulated wall thickness $t_{NT} = 0.34$ nm (the equilibrium distance between two graphite layers), and Young's modulus $E_{NT} = 1$ TPa subsequently calculated by matching the axial stiffness of the SWNT. However, the parameters used in this paper are more reasonable values based on more rationalized theoretical studies and experimental verifications. For example, Yakobson and co-authors concluded from the molecular dynamics simulations of buckling of SWNT that $E_{NT} = 5.5$ TPa, $t_{NT} = 0.066$ nm and $\mu_{NT} = 0.19$. Later, tight-binding simulations lead to an effective wall thickness of 0.074 nm, and Young's modulus of around 5.1 TPa (Zhou et al., 2000). Further evidence was provided by using ab initio energy calculations (Kudin and Scuseria, 2001) which led to $E_{NT} \geqslant 3.0$ TPa and $t_{NT} < 0.094$ nm; followed by local density approximation models (Tu and Ou-Yan, 2002) which reported that $E_{NT} = 4.7$ TPa, $t_{NT} = 0.75$ nm and $\mu_{NT} = 0.34$. Molecular dynamics simulations of axial and torsional deformation (Sears and Batra, 2004) also found $E_{NT} = 2.52$ TPa, $t_{NT} = 0.134$ nm and $\mu_{NT} = 0.21$. Using an equivalent continuum mechanics modelling and experimental verification the authors (Vodenitcharova and Zhang, 2003) found that the rationalized Young's modulus and wall thickness of a carbon SWNT at the atomic scale should have the equivalent values of $E_{NT} = 4.88$ TPa and $t_{NT} = 0.0617$ nm in the frame of continuum mechanics.

2. Continuum mechanics modelling

Consider a straight nanocomposite beam of length L and circular cross section comprising of two materials (Fig. 1): an SWNT of thickness t_{NT}, mid-radius R_{NT}, Young's modulus E_{NT} and Poisson's ratio μ_{NT}, and a matrix of outer radius R_m, Young's modulus E_m and Poisson's ratio μ_m. The beam is being bent in the longitudinal direction by rotating its end sections at a bending angle ψ, which induces a bending moment M. Furthermore, the compressive and tensile longitudinal stresses on both sides of the neutral axis ($\theta = 0°$) flatten the cross section of the nanocomposite beam into an oval shape; the SWNT bends circumferentially and the matrix undergoes in-plane deformation.

The process of longitudinal bending with flattening can be viewed as two superposable stages: (1) the uniform flattening of the straight nanocomposite beam without stretching, and (2) the uniform bending of the nanocomposite beam at a constant degree of ovality. Then, the strain energy of the nanocomposite beam per unit length U is calculated as the sum of the two independent strain energies, in flattening, U_f, and in longitudinal stretching, U_l, where U_f depends on the degree of ovalisation specified by the flattening ratio of the SWNT, ζ_{NT}:

$$\zeta_{NT} = \frac{R_{NT} - R_c}{R_{NT}}, \tag{1}$$

in which R_c is the distance of a point having $\theta = 90°$ on the flattened mid-surface of the SWNT, to the beam neutral axis ($\theta = 0°$). U_l is obviously a function of the curvature of the nanocomposite beam axis, $C = \psi/L$. Therefore, U_l is dependent on ζ_{NT} and C, which are not independent but their values should minimise the strain energy. If C is given, the value of ζ_{NT}, called optimum, is the value that satisfies the condition $\partial U/\partial\zeta_{NT} = 0$. Then, for a given C and calculated optimum ζ_{NT}, the bending moment is calculated as $M = \mathrm{d}U/\mathrm{d}C$.

The following sub-sections will formulate the stress/strain state in both materials during cross-sectional flattening and longitudinal bending. The relationships will then be used for any given curvature C to find the optimum ζ_{NT} and bending moment M. The approach adopted is similar to that described by Calladine (1983) for the Brazier effect in bending of a single macro-tube. However, the present study considers two materials bound together. Moreover, the values of the optimum ζ_{NT} and all other non-dimensional quantities depend on the thickness and material properties of the coating material. The formulae common for the present study and those in Calladine (1983) are given in Appendix A.

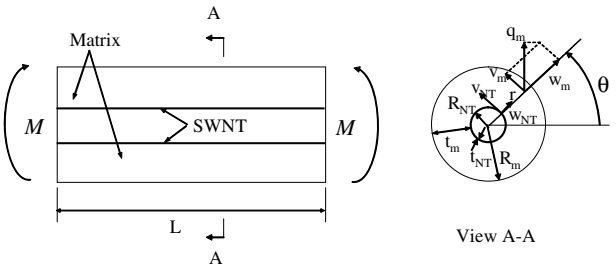

Fig. 1. Nanocomposite beam geometry, where L is the length; R_{NT} and R_m are the original radius of the SWNT and the original outer radius of the matrix, respectively; t_{NT} is the wall thickness of the SWNT; v and w are the radial and circumferential displacements at a material point, 'NT' refers to the SWNT and 'm' refers to the matrix; r is the radial coordinate, θ is the circumferential coordinate and M is the external bending moment.

2.1. Uniform flattening of the nanocomposite beam

First consider the uniform flattening of the nanocomposite beam without stretching, and evaluate the strain energy of a unit length as a bi-material ring. As the cross section remains planar during ovalisation, the radial displacements of the points on the centreline of the SWNT, w_{NT}, can be expressed as in the case of bending of a single tube (Calladine, 1983)

$$w_{\mathrm{NT}} = R_{\mathrm{NT}}\zeta_{\mathrm{NT}}\cos 2\theta. \tag{2}$$

It is obvious that w_{NT} attains a maximum value of $R_{\mathrm{NT}}\zeta_{\mathrm{NT}}$ at $\theta = 0°$ and 180° (outward displacements) and a minimum value of $-R_{\mathrm{NT}}\zeta_{\mathrm{NT}}$ at $\theta = 90°$ and 270° (inward displacements). Consequently, all the stress/strain components and strain energies will be evaluated in terms of w_{NT} and, in view of Eq. (2), in terms of ζ_{NT}.

During flattening, the extreme fibres of the nanocomposite beam at a distance $t_{\mathrm{NT}}/2$ from the centreline of the SWNT, are stretched or compressed in the circumferential direction, following Hooke's law for uniaxial loading. From the simple beam theory the direct strains there, say the tensile ones, $\varepsilon^{\mathrm{e}}_{\theta\theta,\mathrm{NT}}$, are proportional to the curvature change and $t_{\mathrm{NT}}/2$, i.e.,

$$\varepsilon^{\mathrm{e}}_{\theta\theta,\mathrm{NT}} = \frac{t_{\mathrm{NT}}}{2}k_{\theta\theta,\mathrm{NT}} = \frac{3t_{\mathrm{NT}}\zeta_{\mathrm{NT}}}{2R_{\mathrm{NT}}}\cos 2\theta, \tag{3}$$

where the superscript 'e' refers to 'extreme fibres'. $\varepsilon^{\mathrm{e}}_{\theta\theta,\mathrm{NT}}$ above can also be written in terms of the circumferential displacements $v^{\mathrm{e}}_{\mathrm{NT}}$ and the radial displacement $w^{\mathrm{e}}_{\mathrm{NT}}$. It is usual to assume that $w^{\mathrm{e}}_{\mathrm{NT}} = w_{\mathrm{NT}}$ since the ring is thin and the thickness of the SWNT is constant during bending. Therefore,

$$\varepsilon^{\mathrm{e}}_{\theta\theta,\mathrm{NT}} = \frac{1}{R_{\mathrm{NT}} + \frac{t_{\mathrm{NT}}}{2}}\left(\frac{\mathrm{d}v^{\mathrm{e}}_{\mathrm{NT}}}{\mathrm{d}\theta} + w_{\mathrm{NT}}\right). \tag{4}$$

Replacing the left-hand side of Eq. (4) by the right-hand side of Eq. (3) leads to an ordinary differential equation for $v^{\mathrm{e}}_{\mathrm{NT}}$. Solving for the case of no net rotation of the cross section about the longitudinal axis of the beam, one gets

$$v^{\mathrm{e}}_{\mathrm{NT}} = -\frac{1}{2}\left[\left(R_{\mathrm{NT}} + \frac{t_{\mathrm{NT}}}{2}\right)\frac{3t_{\mathrm{NT}}\zeta_{\mathrm{NT}}}{2R_{\mathrm{NT}}} - R_{\mathrm{NT}}\zeta_{\mathrm{NT}}\right]\sin 2\theta. \tag{5}$$

The expressions of w_{NT} and $v^{\mathrm{e}}_{\mathrm{NT}}$ in Eqs. (2) and (5) are subsequently used as boundary conditions for the plane deformation of the matrix.

The next step is to analyse the deformation of the matrix in the plane of the beam cross section. It is reasonable to postulate that the material is in a plane-strain state having two planes of symmetry, $\theta = 0°$ and 90°. It is also expected that at those planes the normal stress components are symmetric and the shear stress components vanish. Therefore one can write

$$\begin{aligned}
\sigma_{rr,\mathrm{m}} &= S_{rr}(\zeta_{\mathrm{NT}}, r)\cos 2\theta,\\
\sigma_{\theta\theta,\mathrm{m}} &= S_{\theta\theta}(\zeta_{\mathrm{NT}}, r)\cos 2\theta,\\
\tau_{r\theta,\mathrm{m}} &= T_{r\theta}(\zeta_{\mathrm{NT}}, r)\sin 2\theta,
\end{aligned} \tag{6}$$

where the subscript 'm' refers to the matrix, σ denotes a normal stress component, τ denotes a shear stress component, r is the radial coordinate of the material point (Fig. 1) and ζ_{NT} is the optimum flattening ratio to be determined.

The stresses in Eq. (6) can be calculated using a conventional method of solid mechanics, e.g., the Airy stress-function method. The stress function can be expressed as a product of two independent functions, in r

and θ. Since the deformation of the cross section has two planes of symmetry, about $\theta = 0°$and 90°, it is expected that the stress function will also be symmetric. Therefore,

$$F = f(\zeta_{\mathrm{NT}}, r)\cos 2\theta. \tag{7}$$

The compatibility equation $\Delta F = 0$ solved for F results in (Boresi and Chong, 1987; Zhang, 2001)

$$F = \left(\overline{A}(\zeta_{\mathrm{NT}})r^2 + \overline{B}(\zeta_{\mathrm{NT}})r^4 + \overline{C}(\zeta_{\mathrm{NT}})\frac{1}{r^2} + \overline{D}(\zeta_{\mathrm{NT}})\right)\cos 2\theta. \tag{8}$$

Consequently, the stress components in Eq. (6) become

$$\begin{aligned}
\sigma_{rr,\mathrm{m}} &= -\left(2\overline{A}(\zeta_{\mathrm{NT}}) + \frac{6\overline{C}(\zeta_{\mathrm{NT}})}{r^4} + \frac{4\overline{D}(\zeta_{\mathrm{NT}})}{r^2}\right)\cos 2\theta,\\
\sigma_{\theta\theta,\mathrm{m}} &= \left(2\overline{A}(\zeta_{\mathrm{NT}}) + 12\overline{B}(\zeta_{\mathrm{NT}})r^2 + \frac{6\overline{C}(\zeta_{\mathrm{NT}})}{r^4}\right)\cos 2\theta,\\
\tau_{r\theta,\mathrm{m}} &= \left(2\overline{A}(\zeta_{\mathrm{NT}}) + 6\overline{B}(\zeta_{\mathrm{NT}})r^2 - \frac{6\overline{C}(\zeta_{\mathrm{NT}})}{r^4} - \frac{2\overline{D}(\zeta_{\mathrm{NT}})}{r^2}\right)\sin 2\theta,\\
\sigma_{zz,\mathrm{m}} &= \mu_{\mathrm{m}}(\sigma_{rr,\mathrm{m}} + \sigma_{\theta\theta,\mathrm{m}}) = 8\mu_{\mathrm{m}}\overline{A}(\zeta_{\mathrm{NT}})\frac{R_{\mathrm{m}}^2}{r^2}\cos 2\theta,
\end{aligned} \tag{9}$$

where $\overline{A}$, $\overline{B}$, $\overline{C}$ and $\overline{D}$ are determined from the boundary conditions. At the free surface of the matrix $r = R_{\mathrm{m}}$, the radial and tangential stresses vanish, i.e.,

$$\begin{aligned}
&\sigma_{rr,\mathrm{m}}(\zeta_{\mathrm{NT}}, R_{\mathrm{m}}, \theta) = 0,\\
&\tau_{r\theta,\mathrm{m}}(\zeta_{\mathrm{NT}}, R_{\mathrm{m}}, \theta) = 0.
\end{aligned} \tag{10}$$

At the interface between the SWNT and the matrix $r = R_{\mathrm{NT}} + t_{\mathrm{NT}}/2$, perfect bond is achieved if the displacements of both materials, therefore the strains, are equal

$$\varepsilon_{\theta\theta,\mathrm{m}}\left(\zeta_{\mathrm{NT}}, R_{\mathrm{NT}} + \frac{t_{\mathrm{NT}}}{2}, \theta\right) = \varepsilon^{\mathrm{e}}_{\theta\theta,\mathrm{NT}}(\zeta_{\mathrm{NT}}, \theta). \tag{11}$$

It is easy to notice that $\overline{B}$ makes the expression of $\tau_{r\theta,\mathrm{m}}$ in Eq. (9) unbound at $r \to \infty$ since $\tau_{r\theta,\mathrm{m}}$ increases with r. However, $\tau_{r\theta,\mathrm{m}}$ is expected to decrease with r and vanish at $r = R_{\mathrm{m}}$; therefore $\overline{B}$ must be 0.

Further, if Eq. (9) is applied to Eq. (10), two of the constants, say $\overline{C}$ and $\overline{D}$, can be expressed in terms of the third constant, $\overline{A}$

$$\begin{aligned}
\overline{C} &= \overline{A}(\zeta_{\mathrm{NT}})R_{\mathrm{m}}^4,\\
\overline{D} &= -2\overline{A}(\zeta_{\mathrm{NT}})R_{\mathrm{m}}^2,
\end{aligned} \tag{12}$$

where $\overline{A}$ can be evaluated from the perfect-bond condition in Eq. (11). However, one first needs to express the strains in the matrix in terms of $\overline{A}$, $\overline{C}$ and $\overline{D}$ by using Eq. (9). Thus, Hooke's law reads

$$\begin{aligned}
\varepsilon_{rr,\mathrm{m}} &= \frac{1+\mu_{\mathrm{m}}}{E_{\mathrm{m}}}[(1-\mu_{\mathrm{m}})\sigma_{rr,\mathrm{m}} - \mu_{\mathrm{m}}\sigma_{\theta\theta,\mathrm{m}}],\\
\varepsilon_{\theta\theta,\mathrm{m}} &= \frac{1+\mu_{\mathrm{m}}}{E_{\mathrm{m}}}[(1-\mu_{\mathrm{m}})\sigma_{\theta\theta,\mathrm{m}} - \mu_{\mathrm{m}}\sigma_{rr,\mathrm{m}}],\\
\gamma_{r\theta,\mathrm{m}} &= \frac{\tau_{r\theta,\mathrm{m}}}{G_{\mathrm{m}}},
\end{aligned} \tag{13}$$

where G_{m} is the matrix shear modulus.

The stresses in Eq. (13) are then replaced by their expressions in Eq. (9) with the constants $\overline{C}$ and $\overline{D}$ defined by Eq. (12). Finally, the condition of a perfect bond in Eq. (11) leads to the expression of $\overline{A}$ as a function of the flattening ratio ζ_{NT}

$$\overline{A} = \frac{3t_{\mathrm{NT}}\zeta_{\mathrm{NT}}}{2R_{\mathrm{NT}}}\frac{E_{\mathrm{m}}}{2(1+\mu_{\mathrm{m}})}\frac{1}{1+3\left(\frac{R_{\mathrm{m}}}{R_{\mathrm{NT}}}\right)^4-4\mu_{\mathrm{m}}\left(\frac{R_{\mathrm{m}}}{R_{\mathrm{NT}}}\right)^2}. \tag{14}$$

Having all the stress components evaluated for a given value of ζ_{NT}, one can readily write the expression of the energy stored in the matrix during uniform ovalisation of a unit length of the nanocomposite beam, $U_{\mathrm{f,m}}$, as

$$U_{\mathrm{f,m}} = \frac{1}{2E_{\mathrm{m}}}\int_{R_{\mathrm{NT}}+t_{\mathrm{NT}}/2}^{R_{\mathrm{m}}}\int_0^{2\pi}\Big[\sigma_{rr,\mathrm{m}}^2+\sigma_{\theta\theta,\mathrm{m}}^2+\sigma_{zz,\mathrm{m}}^2-2\mu_{\mathrm{m}}(\sigma_{rr,\mathrm{m}}\sigma_{\theta\theta,\mathrm{m}}+\sigma_{rr,\mathrm{m}}\sigma_{zz,\mathrm{m}}+\sigma_{\theta\theta,\mathrm{m}}\sigma_{zz,\mathrm{m}}) + 2(1+\mu_{\mathrm{m}})\tau_{r\theta,\mathrm{m}}^2\Big]r\,\mathrm{d}r\,\mathrm{d}\theta. \tag{15}$$

The detailed expression of $U_{\mathrm{f,m}}$ as a function of ζ_{NT} is given in Appendix B at the end of this paper.

To calculate the energy of the nanocomposite beam in uniform longitudinal bending at a constant degree of ovality, the second moment of inertia of the cross section of the matrix should be obtained. For this purpose, one needs to express the displacements in the matrix, w_{m} and v_{m}, as functions of ζ_{NT}. Then, the geometric equations can be employed. For a plane-strain state, the geometric equations become

$$\begin{aligned}
\varepsilon_{rr,\mathrm{m}} &= \frac{\partial w_{\mathrm{m}}}{\partial r},\\
\varepsilon_{\theta\theta,\mathrm{m}} &= \frac{1}{r}\left(\frac{\partial v_{\mathrm{m}}}{\partial\theta}+w_{\mathrm{m}}\right),\\
\varepsilon_{zz,\mathrm{m}} &= 0,\\
\gamma_{r\theta,\mathrm{m}} &= \frac{1}{r}\left(\frac{\partial w_{\mathrm{m}}}{\partial\theta}-w_{\mathrm{m}}\right)+\frac{\partial v_{\mathrm{m}}}{\partial r},\\
\gamma_{rz,\mathrm{m}} &= \gamma_{\theta z,\mathrm{m}} = 0.
\end{aligned} \tag{16}$$

The left-hand side of Eq. (16) can be found by substituting Eqs. (9), (12) and (14) in Eq. (13), and then the displacements w_{m} and v_{m} can be determined by integrating the corresponding strains. The radial displacement w_{m} is the integral of $\varepsilon_{rr,\mathrm{m}}$ over r, which, in conjunction with the boundary condition $w_{\mathrm{m}}(\zeta_{\mathrm{NT}}, R_{\mathrm{NT}}+t_{\mathrm{NT}}/2,\theta) = w_{\mathrm{NT}}(\zeta_{\mathrm{NT}},\theta)$ and Eq. (2), leads to

$$\begin{aligned}
w_{\mathrm{m}} &= W_{\mathrm{m}}(\zeta_{\mathrm{NT}}, r)\cos 2\theta,\\
W_{\mathrm{m}} &= R_{\mathrm{NT}}\zeta_{\mathrm{NT}} - 2A\frac{(1+\mu_{\mathrm{m}})}{E_{\mathrm{m}}}\left[(r-R_{\mathrm{NT}}-t_{\mathrm{NT}}/2)-R_{\mathrm{m}}^4\left(\frac{1}{r^3}-\frac{1}{(R_{\mathrm{NT}}+t_{\mathrm{NT}}/2)^3}\right)\right.\\
&\quad\left.+4(1-\mu_{\mathrm{m}})R_{\mathrm{m}}^2\left(\frac{1}{r}-\frac{1}{R_{\mathrm{NT}}+t_{\mathrm{NT}}/2}\right)\right].
\end{aligned} \tag{17}$$

Next, $\partial v_{\mathrm{m}}/\partial\theta$ is expressed in terms of $\varepsilon_{\theta\theta,\mathrm{m}}$ from Eq. (16) and integrated over θ provided that $v_{\mathrm{m}}(\zeta_{\mathrm{NT}}, R_{\mathrm{NT}}+t_{\mathrm{NT}}/2,\theta) = v_{\mathrm{NT}}^{\mathrm{e}}(\zeta_{\mathrm{NT}},\theta)$ and Eq. (5) are taken into account. Thus, the circumferential displacement v_{m} is found to be

$$
\begin{aligned}
v_{\mathrm{m}} &= V_{\mathrm{m}}(\zeta_{\mathrm{NT}}, r)\sin 2\theta,\\
V_{\mathrm{m}} &= \frac{1}{2}\left\{-R_{\mathrm{NT}}\zeta_{\mathrm{NT}} + 2A\frac{(1+\mu_{\mathrm{m}})}{E_{\mathrm{m}}}\left[2(r - R_{\mathrm{NT}} - t_{\mathrm{NT}}/2) + R_{\mathrm{m}}^4\left(\frac{2}{r^3} + \frac{1}{(R_{\mathrm{NT}} + t_{\mathrm{NT}}/2)^3}\right)\right.\right.\\
&\quad \left.\left. - 4R_{\mathrm{m}}^2\left(\frac{2\mu_{\mathrm{m}} - 1}{r} + \frac{1-\mu_{\mathrm{m}}}{R_{\mathrm{NT}} + t_{\mathrm{NT}}/2}\right)\right]\right\}.
\end{aligned}
\tag{18}
$$

2.2. Uniform bending of the nanocomposite beam at a constant degree of ovality

The second stage of the process of pure bending with flattening is a uniform longitudinal bending of the already-uniformly-ovalized nanocomposite beam. As mentioned before, the strain energy of the nanocomposite beam in longitudinal bending U_{l} depends on the curvature C and the degree of ovalisation ζ_{NT}. It is known that in a plane-strain state the plane deformation is accompanied by some longitudinal stretching so that $\sigma_{zz,\mathrm{m}}$ are non-zero; nevertheless, their values are small compared to the corresponding stresses in longitudinal bending. Thus, the strain energy per unit length of the nanocomposite beam U_{l} can be found by the simple beam theory as

$$
U_{\mathrm{l}} = \frac{1}{2}C^2(EI)_{\mathrm{eff}} = \frac{1}{2}C^2(E_{\mathrm{NT}}I_{\mathrm{NT}} + E_{\mathrm{m}}I_{\mathrm{m}}),
\tag{19}
$$

where I_{eff} is the effective bending stiffness, I_{NT} denotes the second moment of inertia of the SWNT (given by Eq. (A.4)) and I_{m} is the second moment of inertia of the cross section of the matrix.

It is obvious that I_{m} should account for the flattening effect. By definition it is the integral of the product of an elementary area of the cross section, $r\,\mathrm{d}r\,\mathrm{d}\theta$, and the square of the perpendicular distance of that area from the beam neutral axis $\theta = 0°$. Letting η_{m} be the distance of an arbitrary point in the matrix from the beam's neutral axis (Fig. 1), it is clear that

$$
\eta_{\mathrm{m}} = w_{\mathrm{m}}\sin\theta + v_{\mathrm{m}}\cos\theta,
\tag{20}
$$

where w_{m} and v_{m} are already known from Eqs. (17) and (18).

Then, I_{m} becomes

$$
I_{\mathrm{m}} = \int_{R_{\mathrm{NT}}}^{R_{\mathrm{m}}}\int_0^{2\pi}(r\sin\theta + \eta_{\mathrm{m}})^2 r\,\mathrm{d}r\,\mathrm{d}\theta.
\tag{21}
$$

Obviously, I_{m} is a function of ζ_{NT}, whose detailed expression can be found in Appendix B.

Finally, the total strain energy in pure bending of a unit length of the nanocomposite beam is the sum of all strain energies, i.e., in flattening of the SWNT $U_{\mathrm{f,NT}}$ and the matrix $U_{\mathrm{f,m}}$, and in longitudinal bending of the nanocomposite beam U_{l}

$$
U = U_{\mathrm{f,NT}} + U_{\mathrm{f,m}} + U_{\mathrm{l}}.
\tag{22}
$$

The strain energy U is a function of two arguments, C and ζ_{NT}. It follows from the principle of minimum strain energy that the values of C and ζ_{NT} should minimise U. If the beam curvature C is given, then U is a function of ζ_{NT}, and Eq. (22) provides a family of curves, each corresponding to a particular value of ζ_{NT}. The optimum value of ζ_{NT} is the one that makes U minimal, i.e., that satisfies the condition $\partial U/\partial\zeta_{\mathrm{NT}} = 0$. With the optimum ζ_{NT}, $U(C)$ is then minimised with respect to C in order to produce the applied bending moment M, i.e.,

$$
M = \frac{\mathrm{d}U}{\mathrm{d}C}.
\tag{23}
$$

It is convenient to introduce a non-dimensional bending moment m and normalize M with respect to the bending moment $M_{\mathrm{cr},0,\mathrm{NT}}$ that is induced in a circular nanocomposite beam if the compressive stress in the

extreme fibre of the SWNT is equal to the stress that causes uniaxial buckling of the circular SWNT, $\sigma_{cr,0,NT}$ (Eqs. (A.5)–(A.7)). $\sigma_{cr,0,NT}$ can also be used to normalize the longitudinal normal stresses in the SWNT (Eq. (A.8)).

The longitudinal curvature C of the nanocomposite beam is normalized as well and a non-dimensional curvature c is introduced (Eq. A.9). When the curvature increases, it is possible that a value of c is reached, c_{max}, at which m attains a maximum value, m_{max}. Both m_{max} and c_{max} depend on the thicknesses and material properties of both SWNT and matrix.

3. Failure mechanisms

The formulae presented in Section 2 are valid if both SWNT and matrix are perfectly elastic, perfectly bonded and have not failed at any point. With the increase of M, a critical state will be reached at which one of the materials or their interface will fail. There are several types of possible failure mechanisms: (1) *Delamination* or interfacial de-bonding: It is one of the major damage modes which can be caused by shear slip or transverse opening between the two materials. It may be triggered by a pre-existing initial delamination introduced during manufacturing, and will further progress as M increases. (2) *Local buckling* of the SWNT in longitudinal bending: This failure mechanism may be facilitated by an initial bonding defect on the compressive side of the nanocomposite beam. Local buckling of the matrix is also possible when the matrix thickness is small, i.e., a thin film; thicker matrices are more likely to *ripple* on the free surface on the compressive side of the nanocomposite beam. (3) *Fracture* of the matrix: Matrix fracture can occur on the tensile side of the bent nanocomposite beam in longitudinal bending, or at the points of maximum circumferential curvature in flattening of the cross section. (4) *Plastic yielding* of the matrix: When the maximum tensile and compressive stress on the external surface of the matrix reaches its yield stress, plastic deformation occurs.

In this study, we will focus on the local buckling of the SWNT in longitudinal bending. An SWNT is stiff and strong but thin, and it is possible that a critical bending moment is reached when the SWNT buckles locally inward at a location on the compressive side of the beam. It is expected that the surrounding matrix will apply constraints to the onset of local buckling. However, the onset can be conservatively treated by considering the SWNT and matrix separately. It is assumed that the SWNT will buckle locally when the stress in the extreme compressive fibre of the flattened SWNT at the interface with the matrix, $\sigma^{e}_{zz,NT}$, reaches a critical value, $\sigma_{cr,NT}$, given by Eq. (A.10). In a non-dimensional form the criterion for local bifurcation buckling is given by Eq. (A.13). The criterion of local buckling of the SWNT requires an expression for the longitudinal compressive stress in the extreme fibre, $\sigma^{e}_{zz,NT}$. One can use the elementary beam theory and Hooke's law and express the direct longitudinal strain $\varepsilon^{e}_{zz,NT}$ and the corresponding compressive stress $\sigma^{e}_{zz,NT}$ as

$$\begin{aligned} \varepsilon^{e}_{zz,NT} &= -C\left[R_{NT}(1-\zeta_{NT})+\frac{t_{NT}}{2}\right] \\ \sigma^{e}_{zz,NT} &= -E_{NT}C. \end{aligned} \tag{24}$$

If the matrix is thin, one can also expect that it could locally buckle. Similar to the consideration given to the local buckling of the SWNT, Eq. (A.10), the critical buckling stress in the thin film could be written as

$$\sigma_{cr,m} = -\frac{E_m t_m}{\rho_m\sqrt{3(1-\nu_m)}}, \tag{25}$$

where $1/\rho_m$ is the local curvature of the fibre under consideration, say the extreme fibre on the free surface where the compressive strain is the greatest. In order to calculate $1/\rho_m$, the expression of the curvature

change at $\theta = 90°$ can be used. The original curvature of the fibre is $1/R_m$ and the change of curvature becomes

$$k_{\theta\theta,m} = -\frac{1}{R_m^2}\left(w_m + \frac{d^2 w_m}{d\theta^2}\right) = -\frac{3W_m(R_m)}{R_m^2}. \tag{26}$$

Then the curvature of the thin film is

$$\frac{1}{\rho_m} = \frac{R_m - 3W_m(R_m)}{R_m^2}. \tag{27}$$

Knowing the curvature of the thin film, the compressive strain and stress in the extreme fibre at $\theta = 90°$ are then evaluated as

$$\begin{aligned} \varepsilon_{zz,m} &= -\frac{1}{\rho_m}[R_m - W_m(R_m)], \\ \sigma_{zz,m} &= -E_m \varepsilon_{zz,m}. \end{aligned} \tag{28}$$

The thin film will buckle if $\sigma_{zz,m}$ reaches the critical value in Eq. (25).

The stresses in the matrix film can also be normalized with respect to $\sigma_{cr,0,m}$, that is the stress in the matrix calculated from Eq. (25) if ρ_m is replaced by the radius of the fibre, the latter being almost equal to R_m.

4. Results and discussion

The formulae above and in the appendices were applied to a nanocomposite beam comprising of two materials: a carbon SWNT of mid-radius $R_{NT} = 6.66$ Å, Poisson's ratio $\mu_{NT} = 0.19$, thickness $t_{NT} = 0.617$ Å and Young's modulus $E_{NT} = 4.88$ TPa; the latter two parameters were evaluated by the authors (Vodenitcharova and Zhang, 2003). The matrix is titanium having $E_m = 110$ GPa, $\mu_m = 0.33$ (www.efunda.com/materilas/common_matl), tensile yield strength of 140 MPa, ultimate tensile strength of 220 MPa and elongation at break of 54% (www.matweb.com/search/SpecificMaterial). The outer radius of the matrix, R_m, was varied to correspond to the practical range of coating thickness and percentage volume of SWNT in a matrix. Three examples were studied: Example (1) having thickness of the matrix layer $t_m = 5$ Å; Example (2) having $t_m = 15$ Å and Example (3) having $t_m = 63$ Å. Example (1) corresponds to a film of Ti, already produced by Zhang et al. (2000). The second and the third examples, with varied coating thicknesses, are also equivalent to the variation of the percentage volume of SWNTs in a matrix, corresponding to 10.1% and 1.1%, respectively, being common for nanocomposites. This paper considers only a single nanotube embedded into a matrix and the volume percentage of SWNTs can be calculated as the ratio of the volume occupied by the SWNT and the total volume of the nanocomposite material, i.e.,

$$\%\text{SWNT} = \frac{\pi(R_{NT} + t_{NT}/2)^2}{\pi R_m^2}. \tag{29}$$

Initially, the strain energy of a unit length of the beam, $U(\zeta_{NT}, C)$, was calculated according to Eq. (22); the latter provides a family of curves in C and ζ_{NT}. For a particular value of C, U is a function of only one parameter ζ_{NT}, and has a minimum value U_{min} at a value of ζ_{NT} called optimum. First U_{min} and the optimum ζ_{NT} were calculated for a large number of values of C. Then, for the optimum ζ_{NT}, $U(C)$ was minimised with respect to C and the bending moment was estimated as $M = dU/dC$. After that, all quantities of interest were calculated for each C and the corresponding optimum ζ_{NT}, using the formulae in the previous sections and Appendix A.

4.1. Coated SWNT

Let us look at the results for the coated SWNT with $t_m = 5$ Å, i.e., Example (1). An obvious indicator of the stress/strain level in the nanocomposite beam is the direct strain. It was found that in both SWNT and coating, the dominant strains are the direct strains in the longitudinal direction (Fig. 2(a)). As expected, their largest magnitudes are observed at the free surface of the matrix at $\theta = 90°$ and 270°; there the matrix can fracture (on the tensile side) or ripple (on the compressive side). The flattening of the cross section causes circumferential bending of both materials as the direct strains in the circumferential direction are larger at the interface than at the free surface of the coating; however, those strains are smaller than the strains in the longitudinal direction.

The critical direct longitudinal strain $\varepsilon_{cr,NT}$ was also calculated for the considered values of C, Fig. 2(a). It is clear that $\varepsilon_{cr,NT}$ decreases when the curvature C increases. When $\varepsilon_{cr,NT}$ intersects the curve of the actual compressive strains $\varepsilon^e_{zz,NT}$, local buckling of the SWNT initiates, which appears to be the governing failure mode. At local buckling, the non-dimensional curvature c was recorded to be $c = 0.32$ ($C = 52\,800$ mm^{-1}, ψ is around 22.8°); the direct longitudinal strain is $\varepsilon_{zz,m} = \varepsilon^e_{zz,NT} = -3.2\%$ at the interface and $\varepsilon_{zz,m} = -5.8\%$ at the free surface (Table 1).

Fig. 2(b) illustrates the variation of the non-dimensional quantities with the non-dimensional curvature c. The flattening of the nanotube increases with c as the SWNT flattens more than the matrix; at local buckling ζ_{NT} is around 0.14 and ζ_m is 0.074. The critical normal stress in the SWNT along the z-axis, $\sigma_{zz,0,NT}$

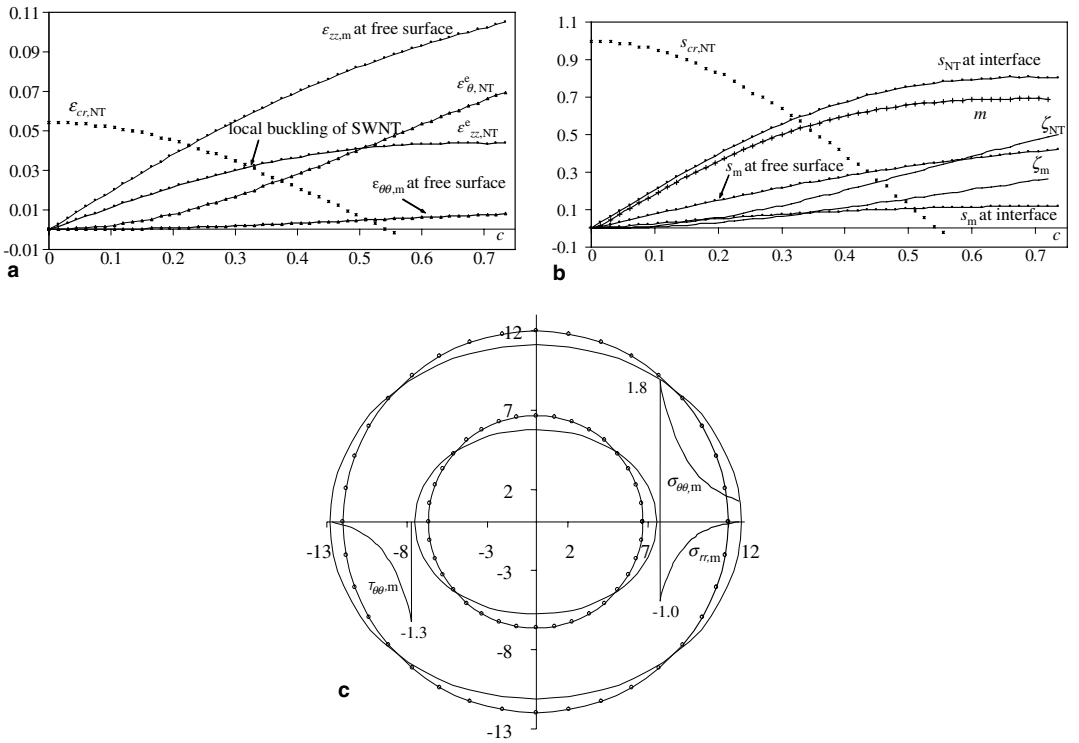

Fig. 2. (a) Direct strains in the SWNT and the matrix (for convenience shown positive), $t_m = 5$ Å. (b) Non-dimensional quantities in the SWNT and matrix (for convenience all stresses shown positive), $t_m = 5$ Å. (c) Cross section of the nanocomposite beam (dimensions are in Å) and stress magnitudes at local buckling (shown in GPa), $t_m = 5$ Å.

Table 1

Example	$t_{\text{film}} = 5$ Å	$t_{\text{film}} = 15$ Å	$t_{\text{film}} = 60$ Å
Curvature at local buckling, c, C	$c = 0.32$, $C = 52\,800$	$c = 0.24$, $C = 38\,900$	$c = 0.063$, $C = 10\,400$
$\varepsilon_{zz,\text{NT}}$ at local buckling	−3.2%	−2.2%	−0.5%
$\varepsilon_{\theta\theta,\text{NT}}$ at local buckling	1.9%	2.6%	4.2%
$\varepsilon_{zz,\text{m}}$ at free surface at local buckling	−5.8%	−8.1%	−6.9%
$\varepsilon_{rr,\text{m}}$ at interface at local buckling	−1.5%	−2.5%	−4.4%
ζ_{NT} at local buckling	0.14	0.19	0.3
ζ_{m} at local buckling	0.074	0.055	0.028
M at local buckling	1.9×10^{-14}	7.9×10^{-14}	1.74×10^{-12}
$M_{\max}$ at $c_{\max}$ and $\zeta_{\max}$	$M_{\max} = 2.5 \times 10^{-14}$, $c_{\max} = 0.71$, $\zeta_{\max} = 0.48$	None	None
$\sigma_{zz,\text{NT}}$ at local buckling	156	108	25.2
$\sigma_{\theta\theta,\text{NT}}$ at local buckling	92.3	128.8	204.4
$\sigma_{zz,\text{m}}$ at interface at local buckling	−3.8	−2.5	−0.5
$\sigma_{zz,\text{m}}$ at free surface at local buckling	−6.5	−8.9	−7.5
$\sigma_{rr,\text{m}}$ at interface at local buckling	−1	−2	−3.6
$\sigma_{\theta\theta,\text{m}}$ at interface at local buckling	1.8	2.3	3.6
$\tau_{r\theta,\text{m}}$ at interface at local buckling	−1.3	−2.1	−3.6

Note: The units in the table are N, mm, GPa.

(Eq. (A.5)), was calculated as −265.9 GPa, and consequently, $M_{zz,0,\text{NT}}$ (Eq. (A.6)) was found to be 3.57×10^{-14} MPa. The bending moment of the nanocomposite beam M increases with c, and at the point of local buckling is 1.9×10^{-14} N mm (in a non-dimensional form, $m = 0.52$). A comparison was made with the bending of the SWNT with no coating, using the model of Vodenitcharova and Zhang (2004). It appears that without the coating the critical bending moment reduces to $M = 1.17 \times 10^{-14}$ N mm at local buckling, but the critical bending angle increases slightly to $\psi = 23.3°$.

The M–c graph (Fig. 2(b)) also shows that M has a maximum value of $M_{\max} = 2.5 \times 10^{-14}$ N mm ($m_{\max} = 0.69$), which is realised at $c = 0.71$ and $\zeta_{\text{NT}} = 0.48$, and is much larger than $M_{\max}$ (1.24×10^{-14} N mm) in bending of an uncoated SWNT. Coating obviously increases the maximum bending capacity of the nanocomposite beam.

The non-dimensional stresses are also increasing functions of c (Fig. 2(b) and Table 1). At the point of local buckling $\sigma_{zz,\text{NT}}$ is large, 156 GPa ($s_{\text{NT}} = 0.59$), at the free surface $\sigma_{zz,\text{m}}$ is only 6.5 GPa ($s_{\text{m}} = 0.23$). It is obvious that the coating material does not share much of the longitudinal stress in the composite beam.

The stresses in the circumferential direction in both materials are smaller than in the longitudinal direction. Their distribution in the matrix at the point of local buckling of the SWNT is shown in Fig. 2(c). It is evident that the maximum stress is attained at the interface where $\sigma_{\theta\theta,\text{m}}$ is 1.8 GPa, and then sharply decreases towards the free surface ($r = R_{\text{m}}$), where $\sigma_{rr,\text{m}}$ and $\tau_{r\theta,\text{m}}$ are zero. The radial normal stress $\sigma_{rr,\text{m}}$ is negative at points $\theta = 0°$ and 180° and its extremum value at the interface is $\sigma_{rr,\text{m}} = -1$ GPa; the corresponding radial strain is $\varepsilon_{rr,\text{m}} = -1.5\%$. In contrast, the matrix at $\theta = 90°$ and 270° is pulled by the SWNT; at the interface $\sigma_{rr,\text{m}} = 1$ GPa and $\varepsilon_{rr,\text{m}} = 1.5\%$. The circumferential direct strain and stress, on the contrary, are tensile at $\theta = 0°$ and 180° and compressive at $\theta = 90°$ and 270°. Their maximum values are at the interface and were found to be $\varepsilon_{\theta\theta,\text{m}} = 1.9\%$ and $\sigma_{\theta\theta,\text{m}} = 1.8$ GPa. Fig. 2(c) also shows the shear stress at points having circumferential coordinates $\theta = 45°$ and 225°, where it attains its extremum value of 1.3 GPa at the interface. The shear stresses in the matrix are zero at the planes of symmetry $\theta = 0°$, 90°, 180° and 270°.

The results above indicate that the radial flexibility of the SWNT leads to a more pronounced deformation of the SWNT while the matrix is less deformed. This makes the SWNT more prone to local buckling and introduces high stresses in the matrix in the vicinity of the interface, which very quickly decrease with the distance towards the free surface of the nanocomposite beam.

4.2. Effect of coating thickness

Similar results were obtained for nanocomposite beams having a SWNT of the same radius but a matrix of thickness $t_m = 15$ Å and 60 Å, which are equivalent to a percentage volume SWNT content of 10.1%, and 1.1%, respectively, according to Eq. (29). The direct strains and non-dimensional quantities in both the SWNT and the matrix are shown in Fig. 3(a) and (b) and Fig. 4(a) and (b). The stress distributions in the beam cross section at the point of local buckling are similar to those in Example (1); their maximum values are given in Table 1.

Some conclusions can be drawn on the influence of the thickness of the coating/matrix layer on the performance of the beam (Fig. 5). It seams that the thicker the coating, the more deformed the SWNT at the same curvature (Fig. 5(a)). Moreover, at the point of local buckling of the SWNT, the nanotube is more deformed if it is embedded in a thick matrix; ζ_{NT} in Example (2) at local buckling is 0.19, while in Example (3) it is 0.3. In contrast, the matrix is less deformed; at local buckling $\zeta_m = 0.055$ in Example (2) and $\zeta_m = 0.028$ in Example (3).

Since ζ_{NT} and c are related, it appears that larger ζ_{NT} leads to lower c. Therefore, the thicker coating makes the nanocomposite beam more prone to local buckling of the SWNT (Fig. 5(b)). In Example (2), local buckling happens at $c = 0.24$ ($C = 38\,900\ \text{mm}^{-1}$, $\psi = 16.8°$) whereas in Example (3), $c = 0.063$ ($C = 10\,400\ \text{mm}^{-1}$, $\psi = 4.5°$). The critical longitudinal strain $\varepsilon_{cr,NT}$ decreases with increasing t_m; it is 2.2% in Example (2) and 0.5% in Example (3). This suggests that the radial flexibility of the SWNT compromises the performance of nanocomposite beams in pure bending and this effect is more pronounced for thicker coating/matrix materials.

The load-bearing capacity M increases with t_m. At local buckling $M = 7.9 \times 10^{-14}$ N mm in Example (2) and 1.74×10^{-12} N mm in Example (3). However, the change in the non-dimensional moment m is negligi-

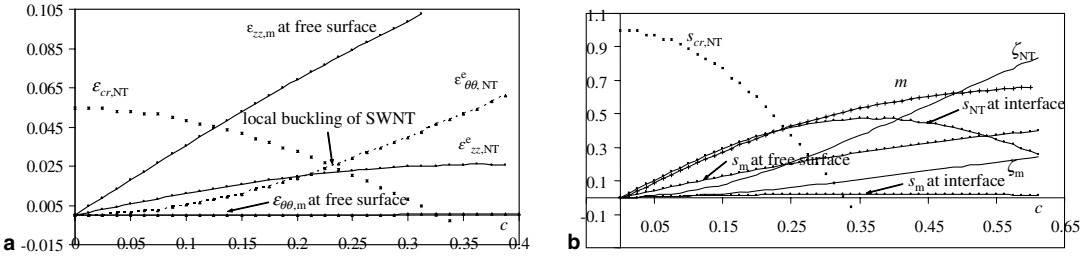

Fig. 3. (a) Strains in the SWNT and matrix, $t_m = 15$ Å. (b) Non-dimensional quantities in the SWNT and matrix (for convenience all stresses shown positive), $t_m = 15$ Å.

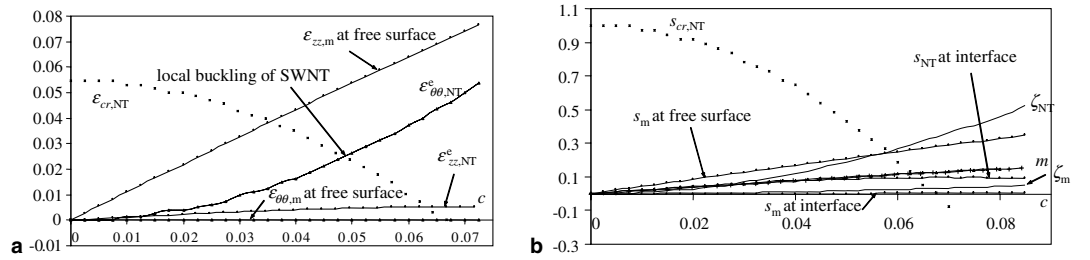

Fig. 4. (a) Strains in the SWNT and matrix for $t_m = 60$ Å. (b) Non-dimensional quantities in the SWNT and matrix (for convenience all stresses shown positive), $t_m = 60$ Å.

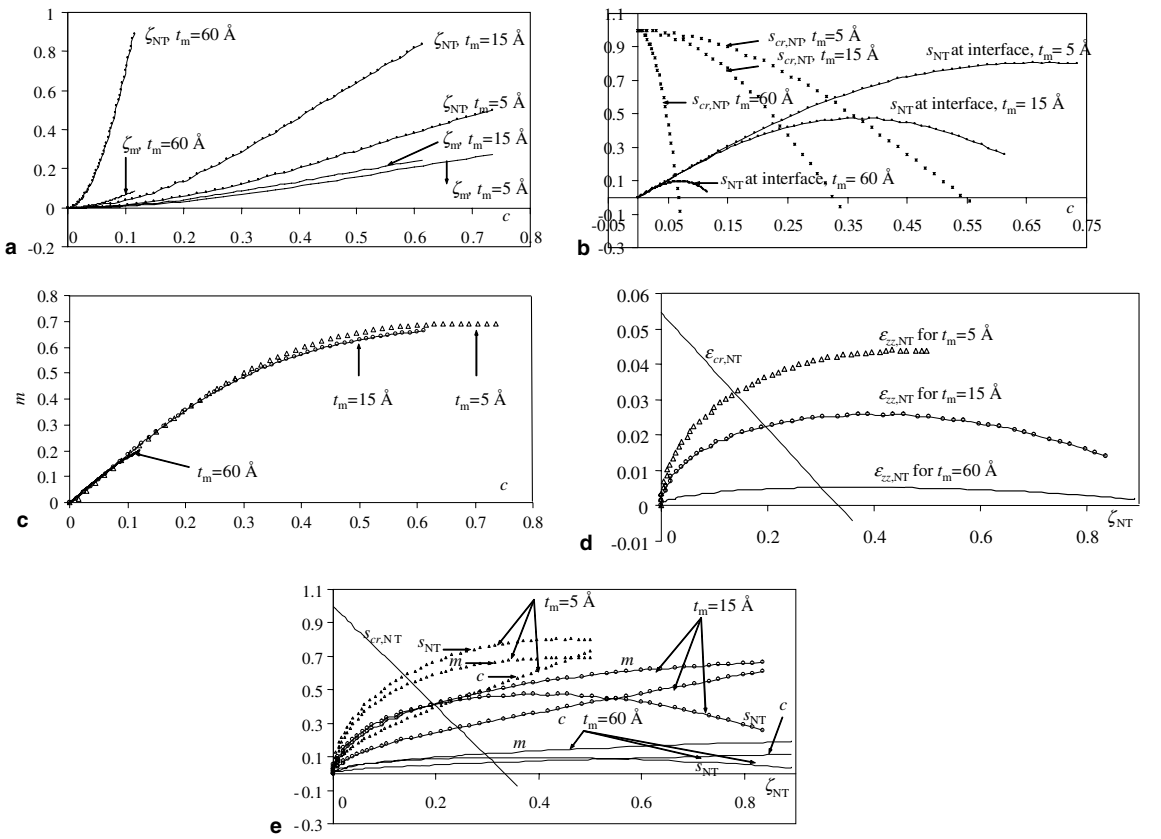

Fig. 5. (a) Variation of the flattening ratios, ζ_{NT} and ζ_m, with the non-dimensional curvature c. (b) Variation of the non-dimensional longitudinal stress in the SWNT, with the non-dimensional curvature c. (c) Variation of the non-dimensional bending moment m with the non-dimensional curvature c. (d) Variation of the longitudinal strains $\varepsilon_{zz,NT}$ with the flattening ratio ζ_{NT}. (e) Variation of non-dimensional quantities with flattening ratio ζ_{NT}.

ble (Fig. 5(c)). Additionally, in thinly-coated SWNT the bending moment M (or m) has a maximum value, while in thickly-coated SWNT it increases monotonically with no maximum point.

All results above seem to indicate that a high volume percentage of SWNT in a composite does not necessary mean a better reinforcement in bending.

Let us see how some stress/strain parameters change with the flattening ratio ζ_{NT} (Figs. 5(d) and (e)). It is evident that the critical longitudinal strain $\varepsilon_{cr,NT}$ is a linear function of ζ_{NT}, i.e., $\varepsilon_{cr,NT} = 0.0544 - 0.0182\zeta_{NT}$. Local buckling occurs at the points of intersection of the line $\varepsilon_{cr,NT}$ with the curves of the actual longitudinal strains $\varepsilon_{zz,NT}$ (Fig. 5(d)). Similar is the dependence of the non-dimensional critical stress s_{cr} on ζ_{NT} (Fig. 5(e)) as $s_{cr} = 1 - 3\zeta_{NT}$, exactly the same as for a SWNT with no matrix. It can be seen in Fig. 5(d) and (e) that while coating decreases the longitudinal strains/stresses at the interface of the two materials, it leads to increased circumferential strains/stresses. Thus, $\varepsilon_{\theta\theta,NT}$ at the interface at local buckling is 2.6% in Example (2), and 4.2% in Example (3); $\sigma_{\theta\theta,m}$ at the interface is 2.3 GPa in Example (2) and 3.6 GPa in Example (3). The radial strains/stresses at local buckling also increase in thicker matrix, as at the interface at $\theta = 0°$ (180°) $\varepsilon_{rr,m}$ is 2.5% and $\sigma_{rr,m}$ is 2 GPa in Example (2) and respectively 4.4% and 3.6 GPa in Example (3). This indicates that the interface between the two materials is more susceptible to an open-mode de-bonding in thicker coating. Further, the shear stress $\tau_{r\theta,m}$ at the interface at $\theta = 45°$

(135°) at the point of local buckling is higher in thicker coating, since it is 2.1 GPa in Example (2) and 3.6 GPa in Example (3). Therefore, thicker nanocomposite beams are more likely to experience interfacial shear delamination than their thinner counterparts.

5. Conclusions

This paper has developed a continuum mechanics model for the uniform bending of a nanocomposite beam of a circular cross section, comprising of a SWNT and a matrix. A two-dimensional deformation problem has been solved for the matrix taking into account the ovalisation of the SWNT cross section. The development of the strain and stress components in both materials has been studied for varying curvatures, flattening ratios and matrix thicknesses. A particular emphasis has been put on the phenomenon of local buckling of the SWNT as a possible failure mode of the nanocomposite beam. Although it has been found that the addition of a matrix to an SWNT increases the load carrying capacity, it also increases the radial deformation of the SWNT at the same bending angle. As a result, thickly-coated SWNTs buckle locally at a lower beam curvature and lower longitudinal strains $\varepsilon_{zz,\mathrm{NT}}$ and stresses $\sigma_{zz,\mathrm{NT}}$. However, the larger degree of flattening of the SWNT, leads to higher strain/stress levels in thicker matrix layers in the plane of the beam cross section.

Acknowledgment

This work was supported by an ARC Discovery Grant.

Appendix A

A circular ring of mid-radius R_{NT} that undergoes non-uniform radial displacements w_{NT}, bends in the circumferential direction. The change of curvature is given as (Calladine, 1983)

$$k_{\theta\theta,\mathrm{NT}} = -\frac{1}{R_{\mathrm{NT}}}\left(\frac{\mathrm{d}^2 w_{\mathrm{NT}}}{\mathrm{d}\theta^2} + w_{\mathrm{NT}}\right), \tag{A.1}$$

which, in view of Eq. (2), leads to

$$k_{\theta\theta,\mathrm{NT}} = \frac{3\zeta_{\mathrm{NT}}}{R_{\mathrm{NT}}}\cos 2\theta. \tag{A.2}$$

The energy of a unit length of the SWNT in flattening, $U_{\mathrm{f,NT}}$, for a given value of the curvature $k_{\theta\theta,\mathrm{NT}}$ in Eq. (A.2), can be expressed as

$$U_{\mathrm{f,NT}} = \frac{1}{2}\int_0^{2\pi} E_{\mathrm{NT}} I_{\mathrm{NT}} k_{\theta\theta,\mathrm{NT}}^2 r\,\mathrm{d}\theta = \frac{3\pi E_{\mathrm{NT}} t_{\mathrm{NT}}^3 \zeta_{\mathrm{NT}}^2}{8R_{\mathrm{NT}}(1-\mu_{\mathrm{NT}}^2)}. \tag{A.3}$$

The second moment of inertia of the already-flattened SWNT reads

$$I_{\mathrm{NT}} = \pi R_{\mathrm{NT}}^3 t_{\mathrm{NT}}\left(1 - \frac{3}{2}\zeta_{\mathrm{NT}} + \frac{5}{8}\zeta_{\mathrm{NT}}^2\right). \tag{A.4}$$

A circular SWNT buckles in uniaxial compression when the compressive stress reaches a critical value of

$$\sigma_{\mathrm{cr},0,\mathrm{NT}} = -\frac{E_{\mathrm{NT}} t_{\mathrm{NT}}}{R_{\mathrm{NT}}\sqrt{3(1-\mu_{\mathrm{NT}}^2)}}. \tag{A.5}$$

If the compressive stress in the extreme fibre of the SWNT is equal to $\sigma_{cr,0,NT}$, then the bending moment induced in the nanocomposite beam (provided that its cross section remains circular) will be

$$M_{cr,0,NT} = \frac{\sigma_{cr,0,NT} I_{eff}}{R_{NT}}. \tag{A.6}$$

A non-dimensional bending moment m can be introduced as

$$m = \frac{M}{M_{cr,0,NT}} \tag{A.7}$$

in a flattened nanocomposite beam m appears to be smaller than one.

The normal stresses in the SWNT can also be normalized with respect to $\sigma_{cr,0,NT}$ and the non-dimensional stresses s can be calculated as

$$s = \frac{\sigma}{\sigma_{cr,0,NT}}, \tag{A.8}$$

where σ denotes any normal stress component in the longitudinal direction.

The longitudinal curvature of the nanocomposite beam axis C can also be normalized

$$c = \frac{1}{2}\frac{CR_{NT}^2\sqrt{3(1-v_{NT}^2)}}{t_{NT}}, \tag{A.9}$$

where c is the non-dimensional curvature.

The criterion of local buckling of the flattened SWNT is similar to that in Eq. (A.5) but R_{NT} is replaced by the radius of local curvature ρ_{NT} of the flattened SWNT cross section at the point of the largest compressive stress, i.e.,

$$\sigma_{cr,NT} = -\frac{E_{NT} t_{NT}}{\rho_{NT}\sqrt{3(1-\mu_{NT}^2)}}, \tag{A.10}$$

where

$$\frac{1}{\rho_{NT}} = \frac{1-3\zeta_{NT}}{R_{NT}}. \tag{A.11}$$

In view of Eqs. (A.5) and (A.10), the non-dimensional critical buckling stress for the SWNT reads

$$s_{cr,NT} = \frac{R_{NT}}{\rho_{NT}}. \tag{A.12}$$

Then, Eq. (A.11) applied to Eq. (A.12) yields $s_{cr,NT} = 1 - 3\zeta_{NT}$ and the criterion for local buckling becomes

$$s = 1 - 3\zeta_{NT}. \tag{A.13}$$

Appendix B

The energy stored in the matrix during uniform ovalisation of a unit length of the nanocomposite beam, can be calculated as the work done by the stresses in a plane-strain state. The expression in Eq. (15) takes the form

$$U_{f,m} = \frac{1}{2E_m}\int\int [u_1 + u_2 + u_3 - 2v_m(u_4 + u_5 + u_6) + 2(1+v_m)u_7] r\,dr\,d\theta, \tag{B.1}$$

where the integration is performed over r, varying from $R_{\mathrm{NT}} + t_{\mathrm{NT}}/2$ to R_{m}, and θ, varying from 0° to 2π. Here u_i, $i = 1$–7, are calculated as

$$
\begin{aligned}
u_1 &= \int\int \sigma_{rr,\mathrm{m}}^2 r\,\mathrm{d}r\,\mathrm{d}\theta \\
&= 2\pi A^2\left\{R_{\mathrm{m}}^2 - \left(R_{\mathrm{NT}} + \frac{t_{\mathrm{NT}}}{2}\right)^2 - 3R_{\mathrm{m}}^8\left(\frac{1}{R_{\mathrm{m}}^6} - \frac{1}{(R_{\mathrm{NT}} + t_{\mathrm{NT}}/2)^6}\right) + 12R_{\mathrm{m}}^6\left(\frac{1}{R_{\mathrm{m}}^4} - \frac{1}{(R_{\mathrm{NT}} + t_{\mathrm{NT}}/2)^4}\right)\right. \\
&\qquad \left. -22R_{\mathrm{m}}^4\left(\frac{1}{R_{\mathrm{m}}^2} - \frac{1}{(R_{\mathrm{m}}^2 + t_{\mathrm{NT}}/2)^2}\right) - 16R_{\mathrm{m}}^2\left[\log R_{\mathrm{m}} - \log\left(R_{\mathrm{NT}} + \frac{t_{\mathrm{NT}}}{2}\right)\right]\right\}, \\
u_2 &= \int\int \sigma_{\theta\theta,\mathrm{m}}^2 r\,\mathrm{d}r\,\mathrm{d}\theta \\
&= 2\pi A^2\left\{\left[R_{\mathrm{m}}^2 - \left(R_{\mathrm{NT}} + \frac{t_{\mathrm{NT}}}{2}\right)^2 - 3R_{\mathrm{m}}^8\left(\frac{1}{R_{\mathrm{m}}^6} - \frac{1}{(R_{\mathrm{NT}} + t_{\mathrm{NT}}/2)^6}\right) - 6R_{\mathrm{m}}^4\left(\frac{1}{R_{\mathrm{m}}^2} - \frac{1}{(R_{\mathrm{m}}^2 + t_{\mathrm{NT}}/2)^2}\right)\right]\right\}, \\
u_3 &= \int\int \sigma_{zz,\mathrm{m}}^2 r\,\mathrm{d}r\,\mathrm{d}\theta = -32\pi\mu_{\mathrm{m}}^2 A^2 R_{\mathrm{m}}^4\left(\frac{1}{R_{\mathrm{m}}^2} - \frac{1}{(R_{\mathrm{m}}^2 + t_{\mathrm{NT}}/2)^2}\right), \\
u_4 &= \int\int \sigma_{rr,\mathrm{m}}\sigma_{\theta\theta,\mathrm{m}} r\,\mathrm{d}r\,\mathrm{d}\theta \\
&= -2\pi A^2\left\{R_{\mathrm{m}}^2 - \left(R_{\mathrm{NT}} + \frac{t_{\mathrm{NT}}}{2}\right)^2 - 3R_{\mathrm{m}}^8\left(\frac{1}{R_{\mathrm{m}}^6} - \frac{1}{(R_{\mathrm{NT}} + t_{\mathrm{NT}}/2)^6}\right) - 6R_{\mathrm{m}}^4\left(\frac{1}{R_{\mathrm{m}}^2} - \frac{1}{(R_{\mathrm{m}}^2 + t_{\mathrm{NT}}/2)^2}\right)\right. \\
&\qquad \left. + 6R_{\mathrm{m}}^6\left(\frac{1}{R_{\mathrm{m}}^4} - \frac{1}{(R_{\mathrm{NT}} + t_{\mathrm{NT}}/2)^4}\right) - 8R_{\mathrm{m}}^2\left[\log R_{\mathrm{m}} - \log\left(R_{\mathrm{NT}} + \frac{t_{\mathrm{NT}}}{2}\right)\right]\right\}, \\
u_5 &= \int\int \sigma_{rr,\mathrm{m}}\sigma_{zz,\mathrm{m}} r\,\mathrm{d}r\,\mathrm{d}\theta \\
&= -4\pi\mu_{\mathrm{m}} A^2\left\{-3R_{\mathrm{m}}^6\left(\frac{1}{R_{\mathrm{m}}^4} - \frac{1}{(R_{\mathrm{NT}} + t_{\mathrm{NT}}/2)^4}\right) + 8R_{\mathrm{m}}^4\left(\frac{1}{R_{\mathrm{m}}^2} - \frac{1}{(R_{\mathrm{m}}^2 + t_{\mathrm{NT}}/2)^2}\right)\right. \\
&\qquad \left. + 4R_{\mathrm{m}}^2\left[\log R_{\mathrm{m}} - \log\left(R_{\mathrm{NT}} + \frac{t_{\mathrm{NT}}}{2}\right)\right]\right\}, \\
u_6 &= \int\int \sigma_{\theta\theta,\mathrm{m}}\sigma_{zz,\mathrm{m}} r\,\mathrm{d}r\,\mathrm{d}\theta \\
&= 4\pi\mu_{\mathrm{m}} A^2\left\{-3R_{\mathrm{m}}^6\left(\frac{1}{R_{\mathrm{m}}^4} - \frac{1}{(R_{\mathrm{NT}} + t_{\mathrm{NT}}/2)^4}\right) + 4R_{\mathrm{m}}^2\left[\log R_{\mathrm{m}} - \log\left(R_{\mathrm{NT}} + \frac{t_{\mathrm{NT}}}{2}\right)\right]\right\}, \\
u_7 &= \int\int \tau_{rr,\mathrm{m}}^2 r\,\mathrm{d}r\,\mathrm{d}\theta \\
&= 8\pi A^2\left\{R_{\mathrm{m}}^2 - \left(R_{\mathrm{NT}} + \frac{t_{\mathrm{NT}}}{2}\right)^2 - 3R_{\mathrm{m}}^8\left(\frac{1}{R_{\mathrm{m}}^6} - \frac{1}{(R_{\mathrm{NT}} + t_{\mathrm{NT}}/2)^6}\right) + 6R_{\mathrm{m}}^6\left(\frac{1}{R_{\mathrm{m}}^4} - \frac{1}{(R_{\mathrm{NT}} + t_{\mathrm{NT}}/2)^4}\right)\right. \\
&\qquad \left. + 2R_{\mathrm{m}}^4\left(\frac{1}{R_{\mathrm{m}}^2} - \frac{1}{(R_{\mathrm{m}}^2 + t_{\mathrm{NT}}/2)^2}\right) - 8R_{\mathrm{m}}^2\left[\log R_{\mathrm{m}} - \log\left(R_{\mathrm{NT}} + \frac{t_{\mathrm{NT}}}{2}\right)\right]\right\}.
\end{aligned}
\tag{B.2}
$$

After performing the integration in Eq. (21), having in mind Eqs. (20), (17) and (18), one gets

$$
\begin{aligned}
I_{\mathrm{m}} &= \pi\left(p_1 + \frac{1}{2}p_2 - p_3\right),\\
p_1 &= \int_{R_{\mathrm{NT}}+t_{\mathrm{NT}}/2}^{R_{\mathrm{m}}}\int_0^{2\pi} r^3\sin^2\theta\,\mathrm{d}r\,\mathrm{d}\theta = \frac{1}{4}\left[R_{\mathrm{m}}^4 - \left(R_{\mathrm{NT}} + \frac{t_{\mathrm{NT}}}{2}\right)^4\right],\\
p_2 &= \int_{R_{\mathrm{NT}}+t_{\mathrm{NT}}/2}^{R_{\mathrm{m}}} r\left(W_{\mathrm{m}}^2 + V_{\mathrm{m}}^2\right)\mathrm{d}r\\
&= \frac{5}{8}\left(R_{\mathrm{NT}}\zeta_{\mathrm{NT}} + C_1H_1\right)^2\left[R_{\mathrm{m}}^2 - \left(R_{\mathrm{NT}} + t_{\mathrm{NT}}/2\right)^2\right] + \left(R_{\mathrm{NT}}\zeta_{\mathrm{NT}} + C_1H_1\right)C_1\left\{-\left[R_{\mathrm{m}}^3 - \left(R_{\mathrm{NT}} + t_{\mathrm{NT}}/2\right)^3\right]\right.\\
&\quad \left. - R_{\mathrm{m}}^4\left(\frac{1}{R_{\mathrm{m}}} - \frac{1}{R_{\mathrm{NT}} + t_{\mathrm{NT}}/2}\right) + 2(-5 + 6\mu_{\mathrm{m}})R_{\mathrm{m}}^2\left[R_{\mathrm{m}} - \left(R_{\mathrm{NT}} + t_{\mathrm{NT}}/2\right)\right]\right\}\\
&\quad + C_1^2\left\{\frac{1}{2}\left[R_{\mathrm{m}}^4 - \left(R_{\mathrm{NT}} + t_{\mathrm{NT}}/2\right)^4\right] - \frac{1}{2}R_{\mathrm{m}}^8\left(\frac{1}{R_{\mathrm{m}}^4} - \frac{1}{\left(R_{\mathrm{NT}} + t_{\mathrm{NT}}/2\right)^4}\right)\right.\\
&\quad \times 4\left[4(1-\mu_{\mathrm{m}})^2 + (2\mu_{\mathrm{m}} - 1)^2\right]R_{\mathrm{m}}^4\left[\log R_{\mathrm{m}} - \log\left(R_{\mathrm{NT}} + t_{\mathrm{NT}}/2\right)\right]\\
&\quad \left. + 2(3 - 4\mu_{\mathrm{m}})R_{\mathrm{m}}^2\left[R_{\mathrm{m}}^2 - \left(R_{\mathrm{NT}} + t_{\mathrm{NT}}/2\right)^2\right] + 2R_{\mathrm{m}}^6\left(\frac{1}{R_{\mathrm{m}}^2} - \frac{1}{\left(R_{\mathrm{NT}} + t_{\mathrm{NT}}/2\right)2}\right)\right\},\\
p_3 &= \int_{R_{\mathrm{NT}}+t_{\mathrm{NT}}/2}^{R_{\mathrm{m}}} r^2\left(W_{\mathrm{m}} + V_{\mathrm{m}}\right)\mathrm{d}r = \frac{1}{2}\left(R_{\mathrm{NT}}\zeta_{\mathrm{NT}} + C_1H_1\right)\left[R_{\mathrm{m}}^3 - \left(R_{\mathrm{NT}} + t_{\mathrm{NT}}/2\right)^3\right]\\
&\quad - 2C_1\left\{\frac{1}{4}\left[R_{\mathrm{m}}^4 - \left(R_{\mathrm{NT}} + t_{\mathrm{NT}}/2\right)^4\right] + \frac{1}{2}(3 - 4\mu_{\mathrm{m}})R_{\mathrm{m}}^2\left[R_{\mathrm{m}}^2 - \left(R_{\mathrm{NT}} + t_{\mathrm{NT}}/2\right)^2\right]\right\},
\end{aligned}
\tag{B.3}
$$

where

$$
\begin{aligned}
C_1 &= \frac{1}{R_{\mathrm{NT}}}\,\frac{\frac{3}{2}t_{\mathrm{NT}}\zeta_{\mathrm{NT}}}{1 + 3\frac{R_{\mathrm{m}}^4}{\left(R_{\mathrm{NT}}+t_{\mathrm{NT}}/2\right)^4} - 4\mu_{\mathrm{m}}\frac{R_{\mathrm{m}}^2}{\left(R_{\mathrm{NT}}+t_{\mathrm{NT}}/2\right)^2}},\\
H_1 &= R_{\mathrm{NT}} + \frac{t_{\mathrm{NT}}}{2} - \frac{R_{\mathrm{m}}^4}{\left(R_{\mathrm{NT}} + \frac{t_{\mathrm{NT}}}{2}\right)^3} + 4(1-\mu_{\mathrm{m}})\frac{R_{\mathrm{m}}^2}{R_{\mathrm{NT}} + \frac{t_{\mathrm{NT}}}{2}}.
\end{aligned}
\tag{B.4}
$$

References

Barber, A.H., Cohen, S.R., Wagner, H.D., 2003. Measurement of carbon nanotube–polymer interfacial strength. Applied Physics Letters 82 (23), 4140.

Barber, A.H., Cohen, S.R., Kenig, S., Wagner, H.D., 2004. Interfacial fracture energy measurements for multi-walled carbon nanotubes pulled from a polymer matrix. Composites Science and Technology 64, 2283–2289.

Boresi, A.P., Chong, K.P., 1987. Elasticity in engineering mechanics. Elsevier Science.

Calladine, C.R., 1983. Theory of shell structures. Cambridge University Press.

Chen, W.X., Tu, J.P., Wang, L.Y., Gan, H.Y., Xu, Z.D., Zhang, X.B., 2003. Tribological application of carbon nanotubes in a metal-based composite coating and composites. Carbon 41, 215–222.

Cooper, C.A., Cohen, S.R., Barber, A.H., Wagner, H.D., 2002. Detachment of nanotubes from a polymer matrix. Applied Physics Letters 81 (20), 3873.

Dai, H., 2002. Carbon nanotubes: opportunities and challenges. Surface Science 500, 218–241.

Gao, G., Cagin, T., Goddard III, W.A., 1998. Energetics, structure, mechanical and vibrational properties of single-walled carbon nanotubes. Nanotechnology 9, 184–191.

Iijima, S., Brabec, C., Maiti, A., Bernholc, J., 1996. Structural flexibility of carbon nanotubes. Journal of Chemical Physics 104 (5), 2089–2092.

Kudin, K.N., Scuseria, G.E., 2001. C_2F, BN and C nanoshell elasticity from *ab initio* computations. Physical Review B 64, 235406.

Lau, K.-T., Hui, D., 2002. Effectiveness of using carbon nanotubes as nano-reinforcements for advanced composite structures. Carbon 40, 1605.

Lau, K.-T., Shi, S.-Q., 2002. Failure mechanisms of carbon nanotube/epoxy composites pretreated in different temperature environments. Carbon 40 (15), 2965–2968.

Liu, Y.J., Chen, X.L., 2003. Evaluations of the effective material properties of carbon nanotube-based composites using a nanoscale representative volume element. Mechanics of Materials 35, 69–81.

Lourie, O., Cox, D.M., Wagner, H.D., 1998. Buckling and collapse of embedded carbon nanotubes. Physical Review Letters 81 (8), 1638–1641.

Mylvaganam, K., Zhang, L.C., 2004a. Chemical bonding in polyethylene–nanotube composites: a quantum mechanics prediction. Journal of Physical Chemistry B 108, 5217–5220.

Mylvaganam, K., Zhang, L.C., 2004b. Important issues in a molecular dynamics simulation for characterising the mechanical properties of carbon nanotubes. Carbon 42, 2025–2032.

Mylvaganam, K., Zhang, L.C., 2004c. Nanotube functionalization and polymer grafting: an *ab-initio* study. Journal of Physical Chemistry B 108, 15009–15012.

Qian, D., Dickey, E.C., Andrews, R., Rantell, T., 2000. Load transfer and deformation mechanisms in carbon nanotube–polystyrene composites. Applied Physics Letters 76 (20), 2868.

Salvetat-Delmotte, J.-P., Rubio, A., 2002. Mechanical properties of carbon nanotubes: a fiber digest for beginners. Carbon 40 (10), 1729–1734.

Schadler, L.S., Giannaris, S.C., Ajayan, P.M., 1998. Load transfer in carbon nanotube epoxy composites. Applied Physics Letters 73 (26), 3842–3844.

Sears, A., Batra, R.C., 2004. Macroscopic properties of carbon nanotubes from molecular-mechanics simulations. Physical Review B 69, 235406.

Shaffer, M., Windle, A.H., 1999. Fabrication and characterization of carbon nanotube/poly(vinyl alcohol) composites. Advanced Materials 11 (11), 937.

Srivastava, D., Menon, M., Cho, K., 1999. Nanoplasticity of single-wall carbon nanotubes under uniaxial compression. Physical Review Letters 83 (15), 2973–2976.

Tai, N.-H., Yeh, M.-K., Liu, J.-H., 2004. Enhancement of the mechanical properties of carbon nanotube/phenolic composites using a carbon nanotube network as the reinforcement. Carbon 42, 2774–2777.

Thostenson, E.T., Chou, T.-W., 2003. On the elastic properties of carbon nanotube-based composites: modelling and characterization. Applied Physics 36, 573.

Thostenson, E.T., Ren, Z., Chou, T.-W., 2001. Advances in the science and technology of carbon nanotubes and their composites: a review. Composites Science and Technology 61, 1899.

Tu, Z.-c., Ou-Yan, Z.-c., 2002. Single-walled and multiwalled carbon nanotubes viewed as elastic tubes with the effective Young's moduli dependent on layer number. Physical Review B 65, 233407.

Vodenitcharova, T., Zhang, L.C., 2003. Effective wall thickness of a single-walled carbon nanotube. Physical Review B 68, 165401.

Vodenitcharova, T., Zhang, L.C., 2004. Mechanism of bending with kinking of a single-walled carbon nanotube. Physical Review B 69, 115410.

Wagner, H.D., Lourie, O., Feldma, Y., Tenne, R., 1998. Stress-induced fragmentation of multiwall carbon nanotubes in a polymer matrix. Applied Physics Letters 72 (2), 188–190.

Yakobson, B.I., Brabec, C.J., Bernholc, J., 1996. Nanomechanics of carbon tubes: instabilities beyond linear response. Physical Review Letters 76 (14), 2511–2514.

Yu, M.F., Dyer, M.J., Ruoff, R.S., 2001. Structure and mechanical flexibility of carbon nanotube ribbons: an atomic-force microscopy study. Journal of Applied Physics 89 (8), 4554–4557.

Zhang, L.C., 2001. Solid mechanics for engineers. Palgrave.

Zhang, Y., Franklin, N.W., Chen, R.J., Dai, H., 2000. Metal coating on suspended carbon nanotubes and its implication to metal–tube interaction. Chemical Physics Letters 331, 35–41.

Zhou, X., Zhou, J., Zhong-can, O.-Y., 2000. Strain energy and Young's modulus of single-wall carbon nanotubes calculated from electronic energy-band theory. Physical Review B 62 (20), 13692.